

Chapter 14

Robust Aerodynamic Design Optimization of Horizontal Axis Wind Turbine Rotors

Marco Caboni, Edmondo Minisci and Michele Sergio Campobasso

Abstract The work reported in this paper deals with the development of a design system for the robust aerodynamic design optimization of horizontal axis wind turbine rotors. The system developed is here used to design a 126-m diameter, three-bladed rotor, featuring minimal sensitivity to uncertainty associated with blade manufacturing tolerances. In particular, the uncertainty affecting the rotor geometry is associated with the radial distributions of blade chord and twist, and the airfoil thickness. In this study, both geometric and operative design variables are treated as part of the optimization. Airfoil aerodynamics and rotor aeroelasticity are predicted by means of XFOIL and FAST codes, respectively, and a novel deterministic method, the Univariate Reduced Quadrature, is used for uncertainty propagation. The optimization is performed by means of a two-stage multi-objective evolution-based algorithm, aiming to maximize the rotor expected annual energy production and minimize its standard deviation. The design optimization is subjected to a single structural constraint associated with the maximum out-of-plane blade tip deflection. The results of this research highlight that a lower sensitivity to uncertainty tied to manufacturing tolerances can be achieved by lowering the angular speed of the rotor.

Keywords Horizontal axis wind turbine design · Multidisciplinary design optimization · Robust design optimization · Uncertainty propagation

M. Caboni (✉)

School of Engineering, University of Glasgow, James Watt Building South,
University Avenue, Glasgow G12 8QQ, UK
e-mail: m.caboni.1@research.gla.ac.uk

E. Minisci

Department of Mechanical and Aerospace Engineering, University of Strathclyde,
75 Montrose Street, Glasgow G1 1XJ, UK
e-mail: edmondo.minisci@strath.ac.uk

M.S. Campobasso

Department of Engineering, Lancaster University, Engineering Building,
Lancaster LA1 4YR, UK
e-mail: m.s.campobasso@lancaster.ac.uk

14.1 Introduction

By the late 20th century, wind power has become one of the most promising new energy sources worldwide, achieving a rapid global growth in installed capacity. Considerable efforts have been put into wind turbine design in order to improve performance and reduce costs, making wind power a competitive energy source. In recent years, several studies have focused on the aerodynamic and structural design optimization of horizontal axis wind turbines (HAWTs) [1–6], encompassing different approaches to increasing the annual energy production (AEP) and reducing the cost of energy. However, an optimized design can become inefficient in the presence of environmental, operation, manufacturing or assembly uncertainties. Therefore, one of the ways to further improve the design of modern wind turbines is to consider the effect of the aforementioned sources of uncertainty throughout the optimization process, leading to the design of more effective devices with minimal sensitivity to uncertainties. The design optimization under uncertainty, aiming to maximize the expected value of one of more objective functions (e.g., AEP), while minimizing the effect of uncertainties, is often denoted by the attribute “robust”. Incorporating sources of uncertainty into a robust optimization process implies the use of a suitable technique for uncertainty propagation, which should keep computational costs affordable while maintaining an acceptable accuracy.

Petrone et al. [7] developed a comprehensive multi-physics computational model to study the impact of wind condition variability, manufacturing tolerances and roughness induced by insect contamination on HAWT aerodynamic performance and noise. In this framework, the Latin Hypercube Sampling (LHS) and the Stochastic Simplex Collocation (SSC) methods were successfully used to propagate uncertainties throughout the computational model. In a more recent work, Petrone et al. [8] developed a system for the robust optimization of HAWT rotors under uncertainty represented by insect contamination. Uncertainty was propagated by means of the SSC method. The proposed design strategy was coupled with a multi-objective genetic algorithm.

Minisci et al. [9] demonstrated a methodology for the aerodynamic optimization of HAWT rotors under geometric uncertainty of the blade geometry caused by manufacturing and assembly tolerances. Chord and twist distributions, and the angular speed of the rotor were included in the optimization process. Uncertainty propagation was conveniently performed by means of the Univariate Reduced Quadrature (URQ) approach [10]. The adopted optimization method was based on a two-stages multi-objective optimization strategy.

The work described in this paper aims to improve the current state-of-art in robust aerodynamic design optimization of HAWT rotors by including the effect of a comprehensive range of geometric uncertainties associated with blade manufacturing tolerances in the design process. In this context, blade chord and twist distributions as well as airfoil thickness are considered affected by uncertainty. Design variables include blade chord and twist distributions, airfoil shape, and the angular speed of the rotor. The URQ method for uncertainty propagation, and the two-stages

multi-objective optimization strategy developed by Minisci et al. [9] are used to carry out the robust design process.

The first part of the paper provides a general description of the optimization system, including: (a) the blade geometric module, (b) the aeroelastic module, (c) the URQ uncertainty propagation method, and (d) the procedure and algorithms used to carry out the optimizations. In the second part, the optimization process set-up is presented in detail, and the obtained results are described and discussed in the third part. A conclusion section summarizes the key findings of this work, and suggests some directions for future developments.

14.2 Optimization System

The integrated design system developed within the framework of this work consists of four main components, including: a blade geometric module defining airfoil shapes and blade chord and twist distributions, an aeroelastic module including airfoil aerodynamics and wind turbine rotor aeroelasticity, an algorithm for uncertainty propagation, and a two-stage multi-objective evolution-based optimizer.

14.2.1 Blade Geometric Module

Blade geometric module defines airfoil shapes and blade chord and twist distributions. The airfoil shape parametrization is achieved through a composite third order Bezier curve. More specifically, airfoil suction and pressure sides are described by four third order Bezier curves joined with C_0 , C_1 and C_2 continuity. This solution provides a flexible airfoil parametrization within the context of the optimization process by actively using a total number of eleven design variables, corresponding to the degrees of freedom of the Bezier curve control points. Figure 14.1 shows the control points of the composite third order Bezier curves used to parametrize the airfoil shape. Along the suction side, points from p_1 to p_4 define the first third order Bezier curve, while points from p_4 to p_7 define the second one. In the pressure side, points from p_7 to p_{10} define the third Bezier curve, and points from p_5 to p_7 define the fourth one. Thus, a total of 13 control points are used.

The leading and the trailing edges (points p_1 and p_7 , respectively) are fixed. The degrees of freedom of the Bezier curve control points are the y -coordinate of point p_6 , and the x - and y -coordinates of points p_2 , p_3 , p_5 , p_{11} , and p_{12} . x and y -coordinates of all the remaining control points are determined by the algorithmic to keep the tangent and the curvature continuity between consecutive Bezier curves.

Blade chord and twist distributions are each defined by four design variables, representing chord and twist at four fixed radial sections. Blade chord and twist distributions are reconstructed by using the MATLAB shape-preserving piecewise cubic (pchip) interpolation function over the four radial stations.

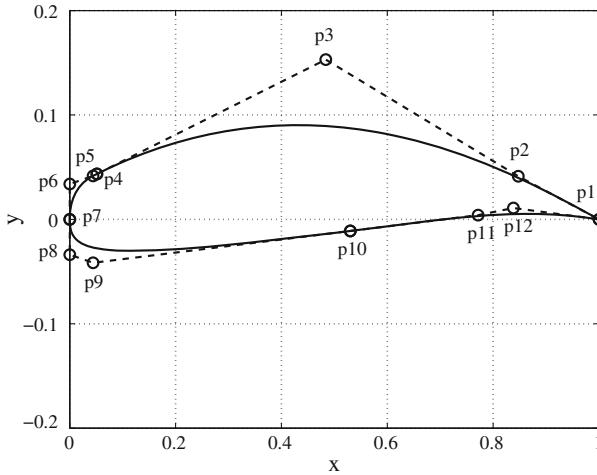


Fig. 14.1 Airfoil shape parametrization through a composite third order Bezier curve

14.2.2 Aeroelastic Module

The aeroelastic module consists of two main components, which are used to compute airfoil aerodynamic loads, as well as rotor power extraction and structural deformations. Lift and drag coefficients of the airfoil, as a function of the Reynolds number and the angle of attack, are calculated using the viscous-inviscid airfoil analysis code XFOIL [11]. XFOIL is a rapid and efficient way of calculating airfoil performance, however it may overestimate lift coefficient, and it does not provide reliable prediction beyond stall. Moreover, two-dimensional (2D) aerodynamic data calculated by means of XFOIL need to be corrected to account for the complex three-dimensional (3D) physics occurring over rotating blades, especially in the stall regime. Based on empirically derived equations, AERODAS [12] provides a method for calculating stall and post-stall lift and drag characteristics of rotating airfoils, using as input a limited amount of pre-stall 2D aerodynamic data of the airfoils used by the turbine under investigation.

The calculation of rotor power extraction and structural deformations is performed by means of the NREL aeroelastic design code FAST [13]. FAST solves the rotor aerodynamics through the AeroDyn code, employing the blade-element momentum (BEM) [14] theory and several corrections including those to account for tip and hub losses, axial induction factors exceeding the maximum theoretical limit of 0.5, and dynamic stall. FAST model uses a linear modal representation to model flexible blades [13]. Blade modes depend on the blade span-variant structural properties, which are tied to the blade external shape and the internal layout of composite laminates.

14.2.3 Method for Uncertainty Propagation

Uncertainty propagation is performed by means of the non intrusive URQ deterministic sampling technique, requiring $2n_u + 1$ evaluations, where n_u is the number of uncertain variables. URQ has a computational cost comparable to that of the linearization method, but allows a higher accuracy. More details about this method can be found in [10], and its validation against Monte Carlo method for wind turbine design can be found in [9].

14.2.4 Optimization Algorithms

Evolutionary Algorithms (EAs) solve optimization problems by making a generation of individuals evolve subject to selection and search operators. In this study, an individual denotes a HAWT rotor configuration, defined by the geometry of the bladed rotor and its rotational speed. This iterative process eventually leads to a population containing the fittest possible individuals (best rotor configuration designs), or individuals who are significantly fitter than those of the starting population. The role of the selection operators is to identify the fittest or most promising individuals of the current population, whereas search operators such as crossover and mutation attempt to generate better offspring starting from suitably selected individuals of the current generation. Each individual is defined by genes, which correspond to design variables in design optimization. The solution of the optimization problems reported in this study is based on a two-stage approach using the Multi-Objective Parzen-based Estimation of Distribution (MOPED) [15] and the Inflationary Differential Evolution Algorithm (IDEA) [16].

MOPED belongs to a subset of EAs and was developed to circumvent certain algorithmic problems of conventional EAs, which can be ineffective when the problem at hand features a high level of interaction among the design variables. This is mainly due to the fact that the recombination operators are likely to disrupt promising sub-structures that may lead to optimal solutions. Additionally, the use of the crossover and mutation operators may result in slow convergence to the solution of the optimization; that is, it may require a large number of generations to obtain very fit individuals. MOPED was developed to circumvent shortfalls of this kind. Its use of statistical tools enables it to preserve promising sub-structures associated with variable interaction from one generation to another (automatic linkage learning). Such statistical tools also replace the crossover and mutation operators of conventional EAs, and they allow a faster convergence of MOPED with respect to the latter class of optimizers. Starting from the individuals of the current population, MOPED builds an approximate probabilistic model of the search space. The role of the crossover and mutation operators is replaced by sampling of this probabilistic model. There exist similar other evolutionary methods that use the aforementioned strategy, and they are called Estimation of Distribution Algorithms (EDAs) [17].

MOPED is a multi-objective optimization EDA for continuous problems that uses the Parzen method [18] to build a probabilistic representation of Pareto solutions, and can handle multivariate dependencies of the variables [15, 19]. MOPED implements the general layout and the selection techniques of the Non-dominated Sorting Genetic Algorithm II (NSGA II) [20], but traditional crossover and mutation search approaches of NSGA-II are replaced by sampling of the Parzen model. NSGA-II was chosen as the base for MOPED mainly due to its simplicity, and also for the excellent results obtained for many diverse optimization problems [21, 22].

The Parzen method utilizes a non-parametric approach to kernel density estimation, and results in an estimator that converges asymptotically to the true Probability Density Function (PDF) over the whole design space. Additionally, when the true PDF is uniformly continuous, the Parzen estimator can also be made uniformly consistent. The Parzen method allocates N_{ind} identical kernels (where N_{ind} is the number of individuals of the current population), each centered on a different element of the sample. A probabilistic model of the promising search space portion is built on the basis of the statistical data provided by the N_{ind} individuals through their kernels, and $\tau_E N_{ind}$ new individuals ($\tau_E \leq 1$) are sampled. The variance of each kernel depends on (i) the location of the individuals in the search space and (ii) the fitness value of these individuals, and its construction leads to values that favor sampling in the neighborhood of the most promising solutions.

The features of MOPED often prevent the true Pareto front from being achieved, particularly when the front is broad and the individuals of the population are spread over different areas, which are far apart from each other in the feasible space. This circumstance has prompted coupling MOPED with another EA, which has better convergence properties. To this aim, the Inflationary Differential Evolution Algorithm (IDEA) [16] has been selected. IDEA was first developed for the design optimization of interplanetary trajectories, and it is an improved variant of the differential evolution (DE) algorithms [16]. The IDEA algorithm is based on a synergistic hybridization of a standard DE algorithm and the strategy behind the monotonic basin hopping (MBH) [23]. The resulting algorithm was shown to outperform both standard DE optimizers and the MBH algorithm in the solution of challenging space trajectory design problems, featuring a multiple funnel-like structure. In this paper, a modified version of IDEA has been used to move the individuals of the approximate Pareto front obtained with MOPED closer to the true front.

The main features of the original IDEA algorithm are reported in [16]. The IDEA algorithm works as follows: a DE process is performed several times and each process is stopped when the population contracts below a predefined threshold. At the end of each DE step, a local search is performed in order to get closer to the local optimum. In the case of non-trivial functions, where there is a high likelihood of converging to local optima, the combined DE/local search is usually iterated several times, performing either a local or a global restart on the basis of a predefined scheduling.

The design optimization presented in this study is constrained. Therefore, the DE step has been modified so that the fitness assessment of the individuals during the DE process also takes into account the constraints. The constraint handling technique used herein is one of the approaches that can be adopted in evolutionary computing,

and is similar to the approach used by MOPED. In the unconstrained DE algorithm [24], and also in the unconstrained IDEA algorithm [16], each parent solution is compared with its offspring, and the solution with a better value of the objective function is passed to the next generation. In the constrained case, on the other hand, when parents and offspring are compared, the solutions are first evaluated in terms of constraint compatibility cp . Its definition is:

$$cp(\mathbf{x}) = \sum_{j=1}^m s_j(\mathbf{x}) \quad (14.1)$$

where \mathbf{x} is the array of design variables, m is the number of constraints, and the constraint factor s_j is:

$$s_j(\mathbf{x}) = \max(g_j(\mathbf{x}), 0) \quad (14.2)$$

The constraint factor equals 0 when the constraint ($g_j(\mathbf{x}) \leq 0$) is satisfied and is strictly positive when the constraint is violated. The solution with the better values of cp is then passed to the next generation. When the cp values of parent and offspring are the same, the selection is performed on the basis of the objective function. In the current implementation, MOPED and IDEA are used sequentially. When MOPED has reached a given number of generations, its final population represents a first and good approximation to the sought Pareto front. Then, clustered sub-populations of such a population are used as initial solutions of the single-objective constraint IDEA optimizer. This algorithm “pushes” the individuals of a sub-population of the MOPED front towards a better local approximation of the sought Pareto front. The resulting two-stage optimizer blends the exploratory capabilities of MOPED (global exploration) and the favorable convergence characteristics of IDEA (exploitation of local information).

14.3 Optimization Set-Up

In this study, two optimizations have been performed: a robust optimization, and a deterministic one (i.e., without considering uncertainties throughout the design process) for comparison purposes.

14.3.1 General Settings

All optimizations performed in this research aimed at maximizing the AEP of a three-bladed HAWT based on the NREL 5-MW reference turbine [25]. The yearly wind distribution was represented by a Weibull distribution with scale parameter of 7 m/s and shape parameter of 2 (Fig. 14.2). The wind turbine was regulated through

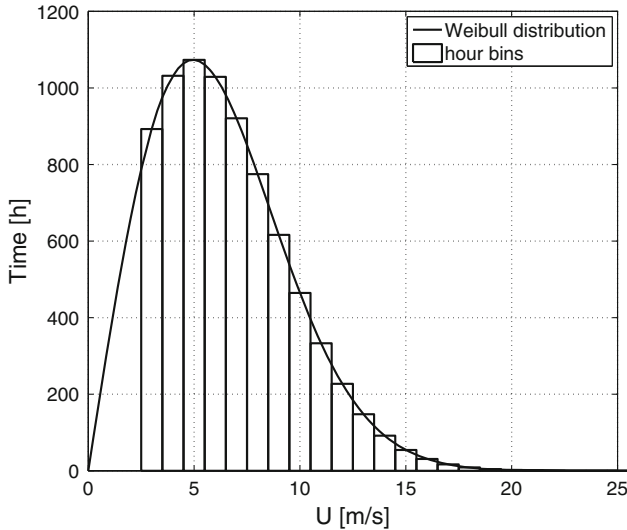


Fig. 14.2 Weibull distribution with scale parameter of 7 m/s and shape parameter of 2, and hour bins for the wind speeds considered between cut-in and cut-out

variable rotational speed before rated wind speed, and variable blade pitch thereafter. Cut-in, rated and cut-out wind speeds were fixed to 3, 12 and 25 m/s, respectively. Blade root radius was set equal to 1.5 m, while blade tip radius was set equal to 63 m. From root to tip, each blade was modeled through seventeen radial sections, including two cylindrical sections near the root, one section transitioning from the last cylindrical section to the first airfoil section, and fourteen airfoil sections over the remainder.

Excluding the cylindrical and transitioning sections near the root, the airfoil distribution along the blade span was defined exclusively by a single aerodynamic shape. Airfoil lift and drag coefficients were computed through XFOIL for a single Reynolds number of $1.2 \cdot 10^7$ over an angle of attack range spanning from -5 to 25° . XFOIL polars were then extended for angles of attack ranging from -180 to 180° , and corrected to account for 3D aerodynamic effects by means of the AERODAS model. In XFOIL, transition from laminar to turbulent flow along the airfoil is simulated by the e^N method, through the parameter NCRIT. For all optimizations reported in this paper, NCRIT was fixed to 9. The airfoil shape and the twist and chord distributions at the airfoil sections were treated as part of the optimization. Lift and drag coefficients of the cylindrical sections near the hub were assumed to be equal to 0 and 0.5, respectively. Lift and drag coefficients for the transitioning section were obtained by interpolating between the neighboring sections. Blade chord and twist distributions were defined at four radial sections r_1 , r_2 , r_3 and r_4 fixed to 11.75, 28.15, 48.65 and 61.6333 m, respectively. The blade shape was parametrized by means of eleven design parameters defining the airfoil shape (x_1 to x_{11}), four design parameters defining the chord distribution (x_{12} to x_{15}), and four design parameters defining the

twist distributions (x_{16} to x_{19}). Wind turbine operating conditions were completely determined by one design variable defining the rotational speed associated with the rated wind speed x_{20} . Indeed, the optimal rotational speed at the given rated wind speed defined the constant optimal tip speed ratio at which the turbine operated between cut-in and rated wind speeds. Thus, the total number of design parameters was equal to 20. Design variables and their ranges of variability are shown in Table 14.1. All optimizations were subject to a structural constraint tied to the maximum out-of-plane blade tip deflection (BTD), which was assumed to be equal to 2/3 of the total clearance in unloaded conditions [3]. Tower diameter was assumed to be constant and equal to 6 m. Rotor overhang, rotor shaft tilt angle, and blade precone angle were fixed to 5.0191 m, 5° , and 2.5° , respectively. Maximum BTD allowed was therefore equal to 6.8 m.

FAST is able to account for flexible bodies, including tower, blades and drive shaft. However, since this work focuses only on the design of bladed rotors, tower and drive shaft deflections were neglected. Moreover, during the optimization process, the adopted hypothesis was to change the internal layout of each turbine in such a

Table 14.1 Range of design variables

x_1	$\in [0.001, 0.2]$	$y(p6)$
x_2	$\in [0.001, 0.2]$	$x(p5)$
x_3	$\in [0.001, 0.2]$	$y(p5)$
x_4	$\in [0.3, 0.6]$	$x(p3)$
x_5	$\in [0.1, 0.5]$	$y(p3)$
x_6	$\in [0.7, 0.9]$	$x(p2)$
x_7	$\in [0.001, 0.1]$	$y(p2)$
x_8	$\in [0.6, 0.8]$	$x(p11)$
x_9	$\in [-0.1, 0.01]$	$y(p11)$
x_{10}	$\in [0.8, 0.99]$	$x(p12)$
x_{11}	$\in [-0.05, 0.1]$	$y(p12)$
x_{12}	$\in [4, 5.5]$ m	$c(r_1)$
x_{13}	$\in [3.5, 5]$ m	$c(r_2)$
x_{14}	$\in [2, 3.5]$ m	$c(r_3)$
x_{15}	$\in [0.5, 2]$ m	$c(r_4)$
x_{16}	$\in [11, 16]^\circ$	$\theta_T(r_1)$
x_{17}	$\in [5, 10]^\circ$	$\theta_T(r_2)$
x_{18}	$\in [0, 5]^\circ$	$\theta_T(r_3)$
x_{19}	$\in [0, 3]^\circ$	$\theta_T(r_4)$
x_{20}	$\in [5, 15]$ RPM	$\Omega(U_{\text{rated}})$

$x(p5)$, $x(p3)$, $x(p2)$, $x(p11)$, and $x(p12)$ represent the x -coordinates of control points $p5$, $p3$, $p2$, $p11$ and $p12$, respectively. $y(p6)$, $y(p5)$, $y(p3)$, $y(p2)$, $y(p11)$ and $y(p12)$ represent the y -coordinates of control points $p6$, $p5$, $p3$, $p2$, $p11$ and $p12$, respectively. $c(r_1)$, $c(r_2)$, $c(r_3)$ and $c(r_4)$ represent the chord length at r_1 , r_2 , r_3 and r_4 , respectively. $\theta_T(r_1)$, $\theta_T(r_2)$, $\theta_T(r_3)$, and $\theta_T(r_4)$ are the twist angles at r_1 , r_2 , r_3 and r_4 , respectively. $\Omega(U_{\text{rated}})$ represents the rotational speed at the rated wind speed

way that the span-variant structural properties remained constant. Therefore, blade modes were considered constant throughout the optimization process.

To avoid intersection between airfoil suction and pressure sides, and more than one change in their curvatures, two constraints were enforced. For practical purposes tied to blade manufacturing, a monotonicity constraint was enforced on both chord and twist distributions.

For both MOPED optimization process, the size of the population have set to 100 and the fitness parameter α_f and the sampling proportion τ_E have been set to 0.5 and 1, respectively. The maximum number of generation was set 100 for the deterministic process and 300 for the robust one. In both IDEA-based optimizations, the weighting factor F and the crossover probability CR have been set to 0.6 and 0.9, respectively. The IDEA search has used a random population of 40 individuals, and has stopped when the population has contracted to 25% of the maximum expansion during the evolution.

14.3.1.1 Robust Design Optimization

The 8 design parameters defining chord and twist distributions as well as the airfoil thickness were assumed to be affected by normally distributed uncertainty. The Gaussian distribution of these parameters was centered at their nominal values. Standard deviations were set to 3° for twist, and 30 cm for chord. At a given radial section, standard deviation for thickness was considered equal to 1% of the chord. The robust optimization described in this paper aimed to maximize the mean value of the AEP and minimize its standard deviation, by varying the twenty aforementioned design variables and propagating the uncertainties affecting the nine variables described above. Robust optimization was achieved by minimizing the following objective functions:

$$F_1 = -\mu_{AEP} \quad (14.3)$$

$$F_2 = \sigma_{AEP}^2 \quad (14.4)$$

where μ_{AEP} is the mean value of the AEP in kWh, and σ_{AEP}^2 is its variance in kWh^2 . The robust optimization was subject to the following constraints:

$$C_1 : \mu_{AEP} \geq 5e6 \quad (14.5)$$

$$C_2 : \sigma_{AEP}^2 \leq 1e11 \quad (14.6)$$

$$C_3 : (\mu_{BTD} + 3 \cdot \sigma_{BTD}) \leq 6.8 \quad (14.7)$$

where μ_{BTD} and σ_{BTD} represent maximum BTD main value and standard deviation in m , respectively. AEP was computed for each turbine by integrating its power curve against the given Weibull distribution. In order to save computational sources, power

curve of each wind turbine was determined through three FAST runs, by interpolating between the power values computed at cut-in wind speed, rated wind speed, and at one intermediate wind speed of 8 m/s. This interpolation was performed by a cubic spine. For each turbine, one additional FAST run was required to determine the maximum BTD. According to Ghedin [3], maximum blade deflections occur when the wind turbine works at rated conditions under a severe gust. In these conditions, the gust occurs so suddenly that the blades cannot be pitched. The gust intensity a wind turbine can withstand depends on its class. The NREL 5-MW reference turbine belongs to the 1A IEC wind class [3], which means it is able to withstand gusts up to 21 % above its rated wind speed. Therefore, maximum BTD was computed at a wind speed equal to 14.52 m/s.

The robust optimization was performed considering identical geometric errors affecting all blades. Each robust analysis performed by means of the URQ technique required 19 computations of AEP, namely 76 FAST runs.

14.3.1.2 Deterministic Design Optimization

Along with the robust optimization, a deterministic optimization was performed. In the deterministic optimization uncertainty sources were not included, and therefore the following objective function was minimized:

$$F_1 = -AEP \quad (14.8)$$

The enforced constraints were:

$$C_1 : AEP \geq 5e6 \quad (14.9)$$

$$C_2 : BTD \leq 6.8 \quad (14.10)$$

14.4 Results and Discussions

14.4.1 Robust Optimization

The robust design optimization problem led to a Pareto front arising from the trade-off between the mean and the standard deviation of AEP. Figure 14.3 shows the URQ Pareto front obtained by means of MOPED. In Fig. 14.3, the performance of a nominal rotor, labeled “URQ ref.,” obtained by using the IDEA local refinement is also represented. Given the final population of the MOPED optimization, the IDEA refinement was performed selecting a sub-population containing a solution with maximum μ_{AEP} , and using it as starting point of the IDEA optimization. This optimization aimed at maximizing μ_{AEP} subject to the constraints (14.5)–(14.7).

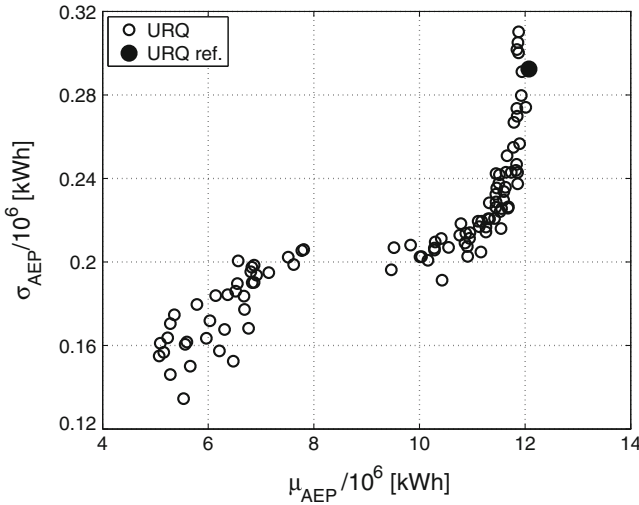


Fig. 14.3 Airfoil shapes of deterministic and robust designs

14.4.2 Robust and Deterministic Optimal Rotors

The deterministic optimization problem led to an optimal rotor which has a nominal AEP of 13.3352 GWh and $\mu_{AEP} = 13.1474$ GWh. This rotor configuration, denoted by “det. opt.,” is compared to the “URQ ref.” rotor, which has a nominal AEP of 12.1435 GWh, and $\mu_{AEP} = 12.0732$ GWh. The AEP standard deviation of the “det. opt.” rotor is $\sigma_{AEP} = 0.2305$ GWh, and is lower than that of the “URQ ref.” rotor, which is equal to $\sigma_{AEP} = 0.2924$ GWh. These results do not meet the usual expectations as the AEP standard deviation of the rotor designed taking into account stochastic geometry errors due to manufacturing tolerances is higher than that of the rotor designed neglecting such errors. The structural constrain on the maximum BTD is the explanation for these results. The robust rotor has a nominal maximum BTD equal to 5.6550 m, and maximum BTD mean and standard deviation equal to 5.6533 and 0.3797 m, respectively. The nominal maximum BTD associated with the deterministic design is equal to 6.788 m, while its mean value and standard deviation are 6.7435 and 0.4915 m, respectively. As can be seen, the constraint (14.7) is verified only for the robust optimization. To demonstrate that the obtained results are strongly influenced by the constraint, a new uncertainty based optimization was performed replacing the reliability constraint (14.7) with the following:

$$C_3 : \mu_{BTD} \leq 6.8 \tag{14.11}$$

The rotor obtained through this new optimization, denoted by “URQ ref. 2”, has a nominal AEP of 13.2751 GWh, $\mu_{AEP} = 13.1263$ GWh and $\sigma_{AEP} = 0.1816$ GWh. The “URQ ref. 2.” rotor has an AEP standard deviation which is lower than that of the “det. opt.” rotor by about 20 %.

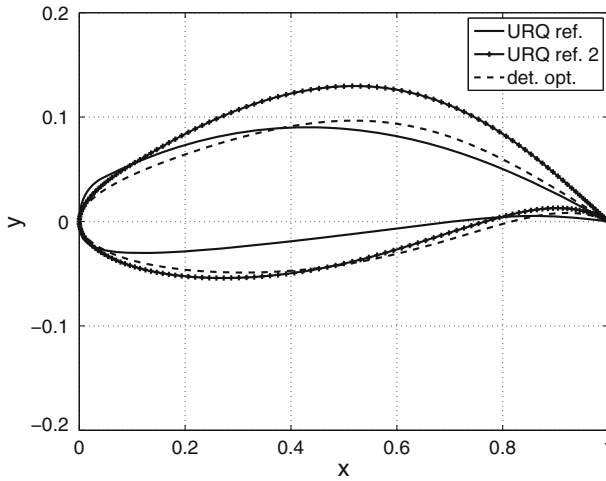


Fig. 14.4 Airfoil shapes of deterministic and robust designs

The airfoil shapes obtained through (i.e., “URQ ref.” and “URQ ref. 2”) and deterministic (i.e. “det. opt.”) optimizations are shown in Fig. 14.4. The radial profiles of the chord c and the pitch angle θ_p of the three rotors are reported in the top left and bottom left subplots, respectively, of Fig. 14.5. Chord distributions of the deterministic and robust designs have the same shape near the root because the cylindrical sections, not treated as part of the optimization, were considered constant.

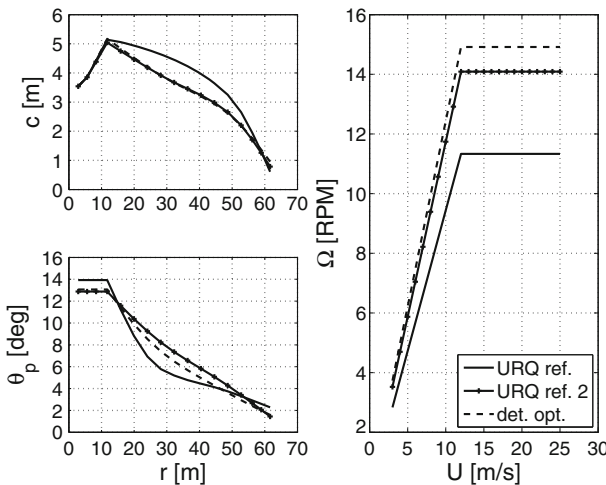


Fig. 14.5 Rotor geometry and control of deterministic and robust designs. *Top left subplot* blade chord c against radius r . *Bottom left subplot* section pitch angle θ_p against radius. *Right subplot* rotational speed Ω against wind speed U

The rotational speed of the three rotors for all considered wind speeds is reported in the right subplot of Fig. 14.5, which highlights that the probabilistically optimized rotors have lower Ω values than the deterministically optimized one.

In light of the above analysis, as it was also reported by Minisci et al. [9], a lower sensitivity of AEP to rotor geometry errors can be achieved by lowering rotational speeds. Further analyses are needed, and have been carrying out by the authors to demonstrate that these results meet the findings obtained in [9]. In this paper it was explained and demonstrated that the reduction of power due to lower circumferential velocities is compensate by an increase of blade aerodynamic loading (i.e., radial lift coefficient distribution), achieved by increasing the angle of attack. This increase is due to the reduced circumferential speed itself, which results in higher values of the relative wind angle. In such conditions, the overall level of angle of attack is in a region where the slope of the angle of attack/lift coefficient curve starts to decrease with respect to the linear part corresponding to lower angles of attack. Therefore, the variation of the lift coefficient caused by a given variation of the angle of attack is smaller for robust rotors.

14.5 Conclusions

A cascade of evolutionary algorithms has been applied to the robust aerodynamic design of a wind turbine rotor to maximize the annual energy production and, at the same time, minimize its variations due to blade manufacturing tolerances. The deterministic URQ sampling approach has been adopted for uncertainty propagation instead of the much more expensive Monte Carlo sampling. The performed robust optimizations and the comparison with the reference deterministic optimization stress the influence of the structural constraint on the achievable results. When the considered constraint limits the magnitude of the mean value of the maximum out-of-plane blade tip deflection, the robust optimization procedure can obtain a rotor producing the same annual energy of the deterministic one, but with a standard deviation which is 20% lower. On the other hand, if a reliability constraint on the maximum out-of-plane blade tip deflection is considered, the average performance of obtained rotors decrease significantly.

Both robust optimization processes performed in this paper confirm that the search for the lower sensitivity to geometry errors is pursued by adopting lower rotational speeds, and further investigations are needed to demonstrate that robustness is actually obtained by moving to a range of higher values of the angle of attack where the slope of the angle of attack/lift coefficient curve is lower than for lower values of the angle of attack.

For this work, low fidelity models such as XFOIL and FAST have been adopted. If the use of low fidelity models allows preliminary design procedures requiring a huge number of model evaluations, on the other hand, the search space should be heavily bounded, to avoid regions of the design space where the (low fidelity) models can not provide correct results. The next step of this work will regard the integration

of the current optimization approach with a multi-fidelity method, which will allow one to achieve a true global design optimization.

References

1. Benini E, Toffolo A (2002) Optimal design of horizontal-axis wind turbines using blade element theory and evolutionary computation. *J Sol Energy Eng* 124(4):357–363
2. Fuglsang P, Madsen HA (1999) Optimization method for wind turbine rotors. *J Wind Eng Ind Aerodyn* 80(1–2):191–206
3. Ghedin F (2010) Structural Design of a 5 MW wind turbine blade equipped with boundary layer suction technology. Master's thesis, Eindhoven University of Technology
4. Vesel RW Jr (2012) Aero-structural optimization of a 5 MW wind turbine rotor. Master's thesis, The Ohio State University
5. Jureczko M, Pawlak M, Mężyk A (2005) Optimisation of wind turbine blades. *J Mater Process Technol* 167(2–3):463–471
6. Xudong W, Shen WZ, Zhu WJ, Sørensen JN, Jin C (2009) Shape optimization of wind turbine blades. *Wind Energy* 12(8):781–803
7. Petrone G, de Nicola C, Quagliarella D, Witteveen J, Iaccarino G (2011) Wind turbine performance analysis under uncertainty. In: Proceeding of the 49th AIAA aerospace sciences meeting including the new horizons forum and aerospace exposition, January 2011
8. Petrone G, de Nicola C, Quagliarella D, Witteveen J, Axerio-Cilies J, Iaccarino G (2011) Wind turbine optimization under uncertainty with high performance computing. In: Proceeding of the 29th AIAA applied aerodynamics conference, June 2011
9. Minisci E, Campobasso MS, Vasile M (2012) Robust aerodynamic design of variable-speed wind turbine rotors. In: Proceeding of the ASME Turbo Expo 2012 technical conference, June 2012
10. Padulo M, Campobasso MS, Guenov MD (2011) A novel uncertainty propagation method for robust aerodynamic design. *AIAA J* 49(3):530–543
11. Drela M (1989) XFOIL: an analysis and design system for low Reynolds number airfoils. In: *Low Reynolds number aerodynamics, Lecture Notes in Engineering*, vol 54. Springer, Heidelberg
12. Spera D (2008) Models of lift and drag coefficients of stalled and unstalled airfoils in wind. *Turbines and Wind Tunnels*
13. Buhl ML Jr, Jonkman JM (2005) FAST user's guide. Technical report NREL/EL-500-38230, National Renewable Energy Laboratory
14. Manwell J, McGowan J, Rogers A (2002) *Wind energy explained. Design and application theory*. Wiley, New York
15. Costa M, Minisci E (2003) MOPED: a multi-objective parzen-based estimation of distribution algorithm. In: *EMO 2003, Faro, Portugal*, Springer, Heidelberg, pp 282–294
16. Vasile M, Minisci E, Locatelli M (2011) An inflationary differential evolution algorithm for space trajectory optimization. *IEEE Trans Evol Comput* 15(2):267–281
17. Lozano JA, Larranaga P, Inza I, Bengoetxea E (2006) *Towards a new evolutionary computation: advances on estimation of distribution algorithms (Studies in fuzziness and soft computing)*. Springer, Heidelberg
18. Fukunaga K (1972) *Introduction to statistical pattern recognition*. Academic Press, New York
19. Avanzini G, Biamonti D, Minisci EA (2003) Minimum-fuel/minimum-time maneuvers of formation flying satellites. *Adv Astronaut Sci* 116:2403–2422
20. Deb K, Pratap A, Agarwal S, Meyarivan T (2002) A fast and elitist multiobjective genetic algorithm: NSGA-II. *IEEE Trans Evol Comput* 6(2):182–197
21. Datta D, Deb K, Fonseca CM, Lobo FG, Conrado PA, Seixas J (2007) Multi-objective evolutionary algorithm for land-use management problem. *Int J Comput Intell Res* 3(4):371–384

22. Deb K (2008) Scope of stationary multi-objective evolutionary optimization: a case study on a hydro-thermal power dispatch problem. *J Glob Optim* 41(4):479–515
23. Leary RH (2000) Global optimization on funneling landscapes. *J Glob Optim* 18(4):367–383
24. Price K, Storn RM, Lampinen JA (2005) *Differential evolution: a practical approach to global optimization*. Springer, Heidelberg
25. Jonkman J, Butterfield S, Musial W, Scott G (2009) Definition of a 5-MW reference wind turbine for offshore system development. Technical report NREL/TP-500-38060, National Renewable Energy Laboratory